Remote Sensing of Environment 255 (2021) 112274

Contents lists available at ScienceDirect

Remote Sensing of Environment

journal homepage: www.elsevier.com/locate/rse

Terrestrial laser scanning intensity captures diurnal variation in leaf water potential

S. Junttila [a,b,*], T. Hölttä [b], E. Puttonen [c], M. Katoh [d], M. Vastaranta [a], H. Kaartinen [c,e], M. Holopainen [b], H. Hyyppä [f]

[a] School of Forest Sciences, University of Eastern Finland, Joensuu 80101, Finland
[b] Department of Forest Sciences, University of Helsinki, Helsinki 00014, Finland
[c] Department of Remote Sensing and Photogrammetry, Finnish Geospatial Research Institute, National Land Survey of Finland (NLS), Masala 02431, Finland
[d] Institute of Mountain Science, Shinshu University, 8304, Minamiminowa-Village, Kamiina-County, Nagano 399-4598, Japan
[e] Department of Geography and Geology, University of Turku, 20500 Turku, Finland
[f] Department of Built Environment, School of Engineering, Aalto University, 02150 Espoo, Finland

ARTICLE INFO

Keywords:
Leaf water potential
Lidar intensity
Terrestrial laser scanning
Diurnal variation
Leaf water content
Drought
Tree health
Plant water dynamics

ABSTRACT

During the past decades, extreme events have become more prevalent and last longer, and as a result drought-induced plant mortality has increased globally. Timely information on plant water dynamics is essential for understanding and anticipating drought-induced plant mortality. Leaf water potential (Ψ_L), which is usually measured destructively, is the most common metric that has been used for decades for measuring water stress. Remote sensing methods have been developed to obtain information on water dynamics from trees and forested landscapes. However, the spatial and temporal resolutions of the existing methods have limited our understanding of the water dynamics and diurnal variation of Ψ_L within single trees. Thus, we investigated the capability of terrestrial laser scanning (TLS) intensity in observing diurnal variation in Ψ_L during a 50-h monitoring period. We aimed to improve the understanding on how large a part of the diurnal variation in Ψ_L can be captured using TLS intensity observations. We found that TLS intensity at the 905 nm wavelength measured from a static position was able to explain 77% of the variation in Ψ_L for three trees of two tree species with a root mean square error of 0.141 MPa. Based on our experiment with three trees, a time series of TLS intensity measurements can be used in detecting changes in Ψ_L, and thus it is worthwhile to expand the investigations to cover a wider range of tree species and forests and further increase our understanding of plant water dynamics at wider spatial and temporal scales.

1. Introduction

Global warming is altering global hydrological cycles, which results in intensified and prolonged droughts causing forest mortality (McDowell and Allen, 2015; Trenberth, 2011). In addition to dry areas becoming dryer, more intense precipitation events occur due to the increased water holding capacity of the warmer air. Altered precipitation patterns and increased evaporation lead to increased drought frequency and severity (Dai, 2013). Water availability has been identified as one of the most significant factors determining the global sensitivity of vegetation productivity to climate variability (Seddon et al., 2016). Major shifts in vegetation patterns may therefore be expected during the following decades, affecting food security and terrestrial carbon uptake (Beer et al., 2010; Wheeler and von Braun, 2013). Understanding the effects of altered water availability requires accurate modelling of plant hydraulics at several scales. The development of such models requires rigorous parameterization and careful testing against observations; multi-scale observations of plant water relations are therefore urgently needed (Konings et al., 2019). A wider availability of plant water measurements would also improve our ability to understand and anticipate drought-induced mortality in plants (Martinez-Vilalta et al., 2019).

Various methods based on remote sensing or in-situ measurements can be used to measure plant and leaf water status. In-situ measurements are either destructive, such as leaf sampling to measure leaf water content or leaf water potential (Ψ_L), or indirect such as the measurement of subtle changes in xylem or stem diameter with linear transducers (De

* Corresponding author at: Department of Forest Sciences, University of Eastern Finland, Yliopistokatu 7, Joensuu 80101, Finland.
E-mail address: samuli.junttila@uef.fi (S. Junttila).

https://doi.org/10.1016/j.rse.2020.112274
Received 21 December 2019; Received in revised form 15 October 2020; Accepted 20 December 2020
Available online 14 January 2021

Swaef et al., 2015) that have been shown to correlate with Ψ_L (Cochard et al., 2002; Dietrich et al., 2018). Stem or leaf water potential can also be measured non-destructively using psychrometers, which utilize a pair of thermocouples to generate wet bulb depression (Guo et al., 2020; Savage et al., 1983). Leaf water potential is one of the most common metrics used in plant physiology and ecology to measure plant water status, as it describes the sensitivity of plant metabolic and transport processes to decreasing soil water availability and atmospheric evaporative demand. It is still mostly measured manually using a Scholander pressure chamber (Scholander et al., 1965), which is laborious to use, requires access to the canopy, and provides only a single reading of the canopy water status in time and space. Also, Ψ_L heterogeneity within the tree canopy due to variation in illumination may decrease measurement accuracy. To further understand the movement of water within the soil-plant-atmosphere continuum and how the water relations of trees and forests are affected by environmental conditions, non-destructive and reproducible measurement methods capable of providing extensive spatiotemporal information on Ψ_L are urgently needed. Measuring the variation in stem or xylem diameter may provide an assessment of the plant water content and Ψ_L of trees (Dietrich et al., 2018) but cannot capture variation in leaf water content within tree canopies and demands a great deal of infrastructure for measuring many trees simultaneously.

Remote sensing methods can be used to estimate leaf water content, from which Ψ_L is estimable, as these two are closely related (Cohen et al., 2005; Cotrozzi et al., 2017; Penuelas et al., 1997). Leaf water potential can be divided into three components according to Eq. (1), where Ψ_π is the osmotic potential (affected by sugars and other dissolved solutes), Ψ_P is the pressure potential that is tightly linked to relative water content, and Ψ_g is the gravitational potential that affects tall trees ($>$ 30 m) in particular. Osmotic potential changes at shorter time intervals due to changes in solute and water content and at longer time intervals due to drought or cold acclimation driven by active osmoregulation. Gravitational potential is constant at a given location in a tree canopy, and thus Ψ_L is mainly controlled by changes in the relative water content of leaves at short time intervals such as days (Kubiske and Abrams, 1991; Olsson and Milthorpe, 1983). Thus, measuring the change in leaf water content may be used as a proxy for estimating Ψ_L.

$$\Psi_L = \Psi_\pi + \Psi_P + \Psi_g \quad (1)$$

Leaf water potential varies during the course of a day and also seasonally. When day temperatures are high during summer, Ψ_L may vary from near 0 before sunrise to ~ -3 MPa at midday when water availability in the soil is not limited (Klepper, 1968; Syvertsen and Levy, 1982). Leaf water potential has also shown vertical variation, for example for peach trees (*Prunus* sp.) with heights of less than 5 m (Olsson and Milthorpe, 1983) and Norway spruce (*Picea abies* (L.) H. Karst.) trees less than 10 m in height (Hellkvist et al., 1974). Lower water potentials were detected higher in the canopy, likely due to the increased transpiration and longer transport distance to the upper parts of the crown (Olsson and Milthorpe, 1983).

Passive remote sensing has been used to measure the variation in leaf water content of individual leaves at close range and of canopies using airborne sensors (Colombo et al., 2008; Danson et al., 1992; Penuelas et al., 1997). The estimation of leaf water content using spectral information is often based on the sensitivity of the shortwave infrared (SWIR) region (1200–2200 nm) to leaf water content (Ceccato et al., 2001). The near-infrared (NIR) region (700–1000 nm) is also sensitive to leaf water content (Penuelas et al., 1997). These methods are, however, dependent on solar illumination and therefore cannot be used at very low sun angles or during night-time to capture the entire diurnal cycle of plant water dynamics. These methods additionally lack the capability to measure the within-tree variation of leaf water content.

The estimation of Ψ_L has been studied using leaf spectroscopy during the last decade, but mainly focusing on grapevines (*Vitis vinifera* L.) (Bei et al., 2011; Rallo et al., 2014; Santos and Kaye, 2009). Cotrozzi et al. (2017) studied the estimation of predawn Ψ_L using spectroscopic measurements from oak tree leaves (*Quercus oleoides* Schltdl. & Cham.) and detected drought-induced changes in predawn Ψ_L. They found that the most significant spectral features for estimating predawn Ψ_L were in the 1400–1470 nm, 1655–1675 nm, 1840–1950 nm, and 2125–2400 nm regions. Rallo et al. (2014) found that vegetation indices combining bands in the NIR (710–760 nm) and SWIR (1550–1650 nm) regions provided the most accurate estimates of Ψ_L. However, such methods are based on single-leaf measurements, which presents a serious issue, since they are prone to error due to the low number of samples and require access to the canopy. Other remote sensing methods used to estimate Ψ_L include thermal remote sensing (Baluja et al., 2012). Cohen et al. (2005) used a thermal camera to assess the Ψ_L of cotton plants (*Gossypium arboreum* L.) and found a strong correlation (coefficient of determination (R^2) = 0.79) between leaf temperature and Ψ_L using a wet reference target. Leaf temperature increased with decreasing Ψ_L. However, methods based on thermal imaging are dependent on sunlight and are thus unsuitable for capturing diurnal variation in Ψ_L.

Terrestrial laser scanning (TLS), is a measurement method that can accurately capture the three-dimensional (3D) structure of trees (Dassot et al., 2011; Krooks et al., 2014). A single TLS scan, which typically takes 3–10 min, produces a point cloud of the surroundings ranging from a few metres to tens of metres. It is repeatable and allows the measurement of multiple tree canopies in high detail. TLS has been widely used to estimate various variables in forests, e.g. forest structural attributes, leaf area index, wood quality, and biomass and to quantify dead wood pools (Antonarakis et al., 2010; Kankare et al., 2013; Liang et al., 2014; Pyörälä et al., 2018; Yrttimaa et al., 2019).

In addition to the 3D structure, TLS measures the strength of the backscattered light at the used wavelength, which in the literature is commonly referred to as intensity (Kaasalainen et al., 2011). Intensity data from TLS may provide additional information on target properties due to its relationship with reflectance at the narrow band of the laser light (Kaasalainen et al., 2009). Terrestrial laser scanning utilizes an active and controlled source of light that is independent of external illumination, reducing the factors that affect the measured spectra and allowing for measurements at any time of day. Dual-wavelength TLS (DW-TLS) and hyperspectral TLS instruments can measure multiple wavelengths, enabling the calculation of spectral ratios similar to passive multispectral imaging. Spectral ratios of TLS intensity can help reduce the leaf structural and incidence angle effects on the measured reflectance (Junttila et al., 2019; Junttila et al., 2016; Nevalainen et al., 2014).

A single intensity measurement consists of the backscattered light under the footprint of the laser, which typically varies around 4–10 mm in a forest environment depending on the distance of the target. Terrestrial laser scanning intensity measurements are complicated by target geometry, which influences the intensity-distance relationship. Terrestrial laser scanning intensity can be described using the radar equation, which states that transmitted power (P_t), aperture area (D), optical efficiency (Q), laser-beam divergence (β), atmospheric transmission losses (T), range (R), and backscattering target cross-section (σ) all affect the received power (P_r):

$$P_r = \frac{P_t D Q}{4\pi\beta^2} T^2 \frac{\sigma}{R^4} \quad (2)$$

where σ comprises target reflectance, geometry, and illuminated area. The power of R is, however, influenced by target size. Planar targets that cover the entire laser footprint cause a stronger backscatter, which diminishes less with distance than linear or blob-like targets due to spherical losses (Wagner et al., 2006). This is an issue with coniferous species, as the needles do not cover even the small footprint of TLS, causing complications in the distance calibration of intensity data (Junttila et al., 2019; Korpela, 2017). Generally, deciduous species do not suffer from the same problem, because leaves fill the laser footprint,

but on the other hand incidence angle effect complicates the interpretation of TLS intensity measurements.

A clear linkage between leaf water content, measured as equivalent water thickness (EWT), and TLS intensity has been shown in several studies (Elsherif et al., 2019a; Gaulton et al., 2013; Junttila et al., 2018; Junttila et al., 2016). Reflectance at the 1550 nm wavelength, which is often utilized in TLS sensors, increases as the leaf water content decreases (Junttila et al., 2016; Rallo et al., 2014). Another wavelength, such as 808 nm or 905 nm, is often employed for accounting leaf structural effects on the measured intensity at 1550 nm, as they are assumed to be less sensitive to leaf water content (Elsherif et al., 2018; Junttila et al., 2018). A nearly linear relationship was found between EWT and a normalized difference index (NDI) calculated from TLS intensity at the 1550 nm and 690 nm wavelengths in a drying experiment in a laboratory environment with five species (Junttila et al., 2016). A combination of the 905 nm and 1550 nm wavelengths showed better accuracy than the 690 nm and 1550 nm wavelengths at predicting EWT in a greenhouse experiment with Norway spruce seedlings (Junttila et al., 2018). Field experiments with DW-TLS have shown promising results for estimating EWT in deciduous species but also low prediction accuracy for coniferous species due to complications arising from distance calibration issues explained above (Elsherif et al., 2019b; Junttila et al., 2019). Elsherif et al. (2019a) investigated the detection of changes in EWT during and after an intense drought event using two observation points in time and DW-TLS data at the 808 nm and 1550 nm wavelengths. However, there is still limited understanding on the capability of TLS intensity in characterizing short-term changes in leaf water content that are related to the diurnal cycle of Ψ_L. Research on monitoring leaf water content changes using TLS has been limited to date.

To increase our understanding of water dynamics and the diurnal variation of Ψ_L within single trees and to overcome the temporal and spatial limitations of passive remote sensing methods and issues arising from the TLS intensity distance calibration of coniferous species, we collected a time series of 15 TLS scans at the 905 nm and 1550 nm wavelengths in the field. We studied and scanned three trees of two species with a nearly constant measurement geometry to determine the diurnal variation of Ψ_L during a 50-h time period coupled with destructive leaf measurements and radial stem diameter measurements. As we cannot measure pressure directly, Ψ_L estimation is based on the well-established theory that a change in leaf water content is the main driver of change in Ψ_L during short time intervals such as days. Our main research question was to investigate how large a part of the diurnal variation in Ψ_L may be captured using TLS intensity observations based on the known correlation between leaf water content, Ψ_L, and TLS intensity at the 905 nm and 1550 nm wavelengths. Based on existing knowledge, we hypothesized that a correlation exists between the measured intensity and Ψ_L. This research contributes to increasing the understanding of tree water dynamics and to the development of novel methods to measure and monitor it.

2. Material and methods

We measured two Scots pines (*Pinus sylvestris* L.) and one silver birch (*Betula pendula* Roth) (Table 1) during a 50-h monitoring period from the 29th to the 31st of July 2019 at the Station for Measuring Ecosystem-Atmosphere Relations (SMEAR II) at Hyytiälä Forest Research Station in Juupajoki, Finland (61°46′ N, 24°17′ E, 170 m a.s.l.) (Table 1). The investigated trees were growing in a 57-year-old Scots pine stand with combinations of silver birch, Norway spruce (*Picea abies* (L.) Karst.), rowan (*Sorbus aucuparia* L.), European aspen (*Populus tremula* L.), and common juniper (*Juniperus communis* L.). The trees were located around a multi-storey measurement tower enabling the collection of observations from the tree crowns during the investigation period.

Table 1
Diameters at breast height (DBH) and heights of the investigated trees.

	Scots pine 1	Scots pine 2	Silver birch
DBH (cm)	22.5	19.8	20.1
Height (m)	18.9	19.5	20.6

Radial stem variation of the trees was measured with point dendrometers, i.e. linear variable displacement transducers (model AX/5.0/S, Solartron Inc. West Sussex, U.K.) at a height of 1.5 m. The dendrometers measured the radial variation of the stem and xylem separately. The xylem diameter changes due to reversible changes in xylem content, while the stem diameter changes due to both reversible changes in stem water content and due to irreversible cell enlargement associated with cambial growth (Chan et al., 2016; Dietrich et al., 2018). As the investigation period was late summer, the cell enlargement phase in the cambial growth of the stem had nearly ceased (see Chan et al., 2016 for the phenology of growth at the site). The radial stem measurements were recorded continuously at a one-minute time resolution.

Environmental variables, such as temperature, relative humidity, wind speed, wind direction, and the amount of incoming thermal radiation, were measured from a measurement tower located ca. 50 m from the measurement site (Fig. 1). The measurements were conducted at one-minute intervals. No precipitation occurred during the investigation period and neither were any dew events observed at the time of the measurements. Soil water potential was simultaneously measured with tensiometers (EQ2 Equitensiometer, Delta-T) combined to pressure transducers (TR2000A, Trans Instruments) at the depths of 5 and 15 cm at 15-min intervals. The data described here are openly accessible from the SMEAR station database (https://avaa.tdata.fi/web/smart/smear).

2.1. Leaf water potential measurements

Leaf water potential was measured at 9 time intervals during the monitoring period (Appendix 1). The top of the tree canopies was divided into three height bins for Ψ_L measurements to ensure a reliable reference for entire tree canopies: the top 2 m, 2–4 m from the top, and 4–6 m from the top. The Ψ_L samples were collected immediately after the TLS measurements. Each sample consisted of four needles or leaves that were collected in air tight plastic bags that were filled with moist air, stored in a dark and cool bag, and carried immediately to the nearby laboratory, where Ψ_L was measured using a Scholander pressure chamber (PMS-1000; PMS Instruments, Albany, OR, USA). Each Ψ_L measurement was the mean of the four samples. The Ψ_L samples were collected in approximately five minutes and the measurement of Ψ_L took approximately 15 min for all the samples of a single canopy.

As a dependency between canopy water status and radial stem diameter variation is known to occur (Dietrich et al., 2018), we created

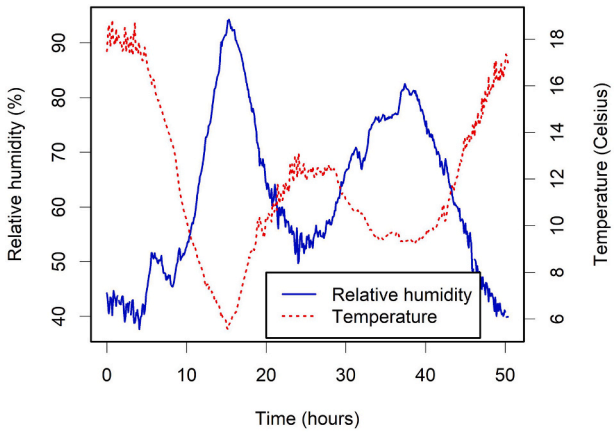

Fig. 1. Variation of temperature and relative humidity during the monitoring period. The measurements were started at 13:00 on the 29th of July and ended at 15:00 on the 31st of July 2019.

linear regression models between Ψ_L and the radial stem diameter variation for each tree to increase the number of Ψ_L data points. Using these models, we predicted Ψ_L for each 15 time points of the TLS data. Because a lag occurs in the change in radial stem diameter after a change in Ψ_L, we used a lag in creating the regression models (Sevanto et al., 2002). The predicted Ψ_L is abbreviated as $\Psi_{P\text{-}L}$ in the text.

2.2. TLS measurements

The TLS measurements were started at 13:00 on the 29th of July 2019 and ended at 15:00 in the afternoon two days later. During this monitoring period, the trees were scanned 15 times using two scanners utilizing wavelengths at 905 nm and 1550 nm (see Appendix 1 for accurate timings). Each tree was measured with a single TLS scan subsequently with both scanners from a fixed position with clear visibility to the tree crown to avoid occlusion caused by other trees. Each tree had their own scanning position and the distance to the trees varied from 11 m to 13 m. The time difference between the consecutive two scans was approximately 15 min and one round of TLS scans (all three trees) took about one hour. The scanners used were a FARO X330 (FARO Europe GmbH & Co. KG, Korntal-Münchingen, Germany), which operates at 1550 nm, and a Trimble TX5 (Trimble Inc., Sunnyvale, CA, USA) operating at the 905 nm wavelength. These scanners have similar technical specifications: a beam divergence of 0.19 mrad, a max scan rate of 976 kHz, and intensity recording to a digital number (−2048 to 2033). The beam diameter at output differs slightly, with FARO X330 having a beam diameter of 2.25 mm and the Trimble TX5 a beam diameter of 3 mm. Both scanners utilize phase shifting range measurements. The scanners have the same boxing; thus, the viewing angle is the same between the scanners. Both scanner resolutions were set to 0.5, resulting in a vertical spacing of 3.07 mm at a 10-m distance; the quality parameter was set to 2× (i.e. two measurements were made for each point and the resulting value was the mean of the two). We placed 11 target spheres (each with a diameter of 145 mm) around the measurement tower for further scan registration. A Lambertian Spectralon reflectance panel (Labsphere, North Sutton, NH, USA) with a nominal reflectance of 40% was used as a reference target at a constant distance to normalize the laser intensity of each scan.

2.3. Point cloud processing

The point clouds from each measurement location were co-registered to a common arbitrary coordination system using the external sphere targets as reference points. The registration was performed in FARO Scene point cloud processing software. Each tree was then manually delineated from the individual point clouds using the CloudCompare software package (version 2.10) (Dewez et al., 2016). The calibration of intensity was conducted to reduce variation caused by factors such as temperature and distance. The intensity correction workflow followed the procedure presented in Junttila et al. (2019), which included distance and logarithmic corrections and the normalization of intensity with a reflectance panel with known reflectance. The intensity measured from the reference panel showed a standard deviation between 10 and 13 in raw intensity values. The distance correction was performed using a 10th degree polynomial function that was modelled with empirical data concerning the intensity and distance of the scanner (see Appendix 1 for model parameters). The raw intensity scale of the scanner was found to be logarithmic. Thus, a linearization of the intensity scale was necessary using empirical relationships between reflectance and raw intensity. Further details are provided in Junttila et al. (2019).

2.4. Point cloud segmentation

Each tree canopy was segmented from the point clouds to mainly include needle or leaf points into the analysis. Segmentation was based on a minimum height that was determined visually. The minimum heights that were used to segment the canopies were 9.9 m, 11.5 m, and 10 m, for pine 1, pine 2, and birch, respectively. We included all the points from the canopy into the analysis to avoid interfering with the intensity data distribution at the tree level and to ensure consistency of the data between subsequent measurements of the time series. Thus, no classification to branch and needle or leaf points was carried out. Based on a mean of a random sample of 15,000 points, the birch leaf points showed a calibrated intensity of 0.56 (905 nm) and 0.18 (1550 nm), while branch points had an intensity of 0.48 (905 nm) and 0.28 (1550 nm). The pine needle points had an intensity of 0.31 (905 nm) and 0.12 (1550 nm), and the stem points intensity of 0.45 (905 nm) and 0.37 (1550 nm). The number of points in the resulting point clouds that were used in the analysis varied between 220,000 and 450,000 between the trees and observation times.

2.5. Explanatory intensity metrics

A variety of intensity metrics was calculated for each segmented point cloud (Table 2). These metrics describe the distribution of intensity values within a given point cloud at different wavelengths. The metrics were calculated for the 905 and 1550 nm wavelengths separately. As the calculation of NDI for single 3D points was complicated due to slight movements of the branches between consecutive scans, NDI was calculated based on the distribution of intensity values in the canopy. The calculation of NDI was performed using percentiles (10th, 20th, 30th… 90th) and means of the 905 nm and 1550 nm wavelengths (Eq. (3)). All the intensity metrics are shown in Table 2.

$$NDI = \frac{I_{905} - I_{1550}}{I_{905} + I_{1550}} \quad (3)$$

2.6. Statistical analysis

Student's two-sided *t*-tests were used to assess the difference in Ψ_L at different heights. Linear regression modelling was used to assess the relationships between the intensity metrics and Ψ_L. We used reduced major axis regression (model 2 regression), because both variables contain measurement error (Davis and Sampson, 1986). Regression models were created using both the measured and predicted Ψ_L as dependent variables. Normality of the data was tested using the Shapiro-Wilkinson test (Hanusz and Tarasińska, 2015). The coefficient of determination (R^2) and root-mean-square-error (RMSE) were calculated to assess the estimation accuracy of the intensity variables. All of the statistical analyses were carried out within the R package (R Core Team, 2015).

Table 2
Description of the calculated intensity metrics. In the table, i denotes the wavelength followed by the name of the metric. For example "1550_mean" means average intensity at the 1550 nm wavelength. Respectively, normalized difference index (NDI) metrics are followed by the percentile used in the calculation of NDI. For example, "NDI_p20" means the metric has been calculated using the 20th percentile of the 905 nm and 1550 nm wavelengths).

Metric	Description
i_mean	Average intensity
i_std	Standard deviation of intensity
i_p10, i_p20, … i_p90	Multiple-of-10 percentiles (10th through 90th) of the intensity distribution
i_max	Maximum intensity
i_min	Minimum intensity
i_kur	Kurtosis of the intensity distribution (Davies and Goldsmith, 1976)
i_ske	Skewness of the intensity distribution (Davies and Goldsmith, 1976)
i_entropy	Shannon diversity index (entropy) of the intensity distribution (Shannon, 2001)
i_range	Difference between maximum and minimum intensity
i_D05, i_D25, i_D50, i_D75	Density variables: the 95th percentile divided by the 5th, 25th, 50th, and 75th percentiles, respectively.

3. Results

3.1. Variation in leaf water potential based on the Scholander pressure chamber

The lowest Ψ_L values were observed on the day the measurements were begun (Fig. 2). Fig. 2 shows a minor decreasing trend in Ψ_L higher in the tree for the silver birch, but no significant differences in Ψ_L between the different height layers during the monitoring period. Soil water potential varied between −0.05 and −0.08 MPa at the 15-cm depth and between −0.15 MPa and −0.21 MPa at the 5-cm depth.

3.2. Leaf water potential prediction based on stem diameter measurements

A strong linear relationship was observed between Ψ_L and stem diameter variation for each tree (Fig. 3). The strongest relationship was found using a 90-min time lag between the Ψ_L and stem diameter measurement.

3.3. Assessing the relationships between leaf water potential and intensity metrics

The intensity metrics explained a significant proportion of the variation in Ψ_L (Fig. 4). The best-predicting TLS intensity variables explained 70%, 71%, and 77% of the variation in Ψ_L in pine 1, pine 2, and the birch, respectively (Table 3). Generally, the strongest predictors were mainly distribution features of the 905 nm wavelength, but the distribution of 1550 nm showed similar explanatory power for pine 1. The D25 intensity feature of the 905 nm wavelength explained 77% of the variation in Ψ_L with observations from all of the trees in the prediction model. However, the distribution of intensity metrics using

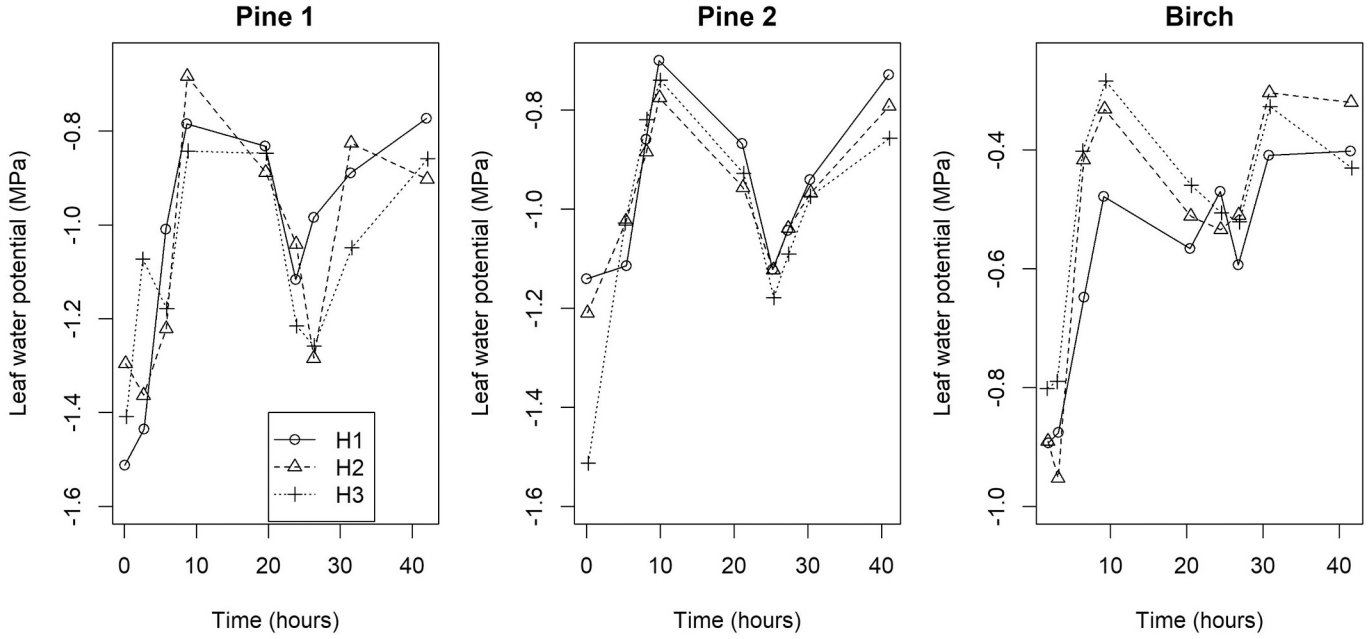

Fig. 2. Variation in leaf water potential (Ψ_L) at different heights during the monitoring period ($n = 4$ for each point, average standard deviation was 0.16 MPa). H1 denotes the top 2 m of height, H2 the top 2–4 m of height, and H3 the top 4–6 m of height. The measurements were started at 13:00 on the 29th of July and ended at 15:00 on the 31st of July 2019.

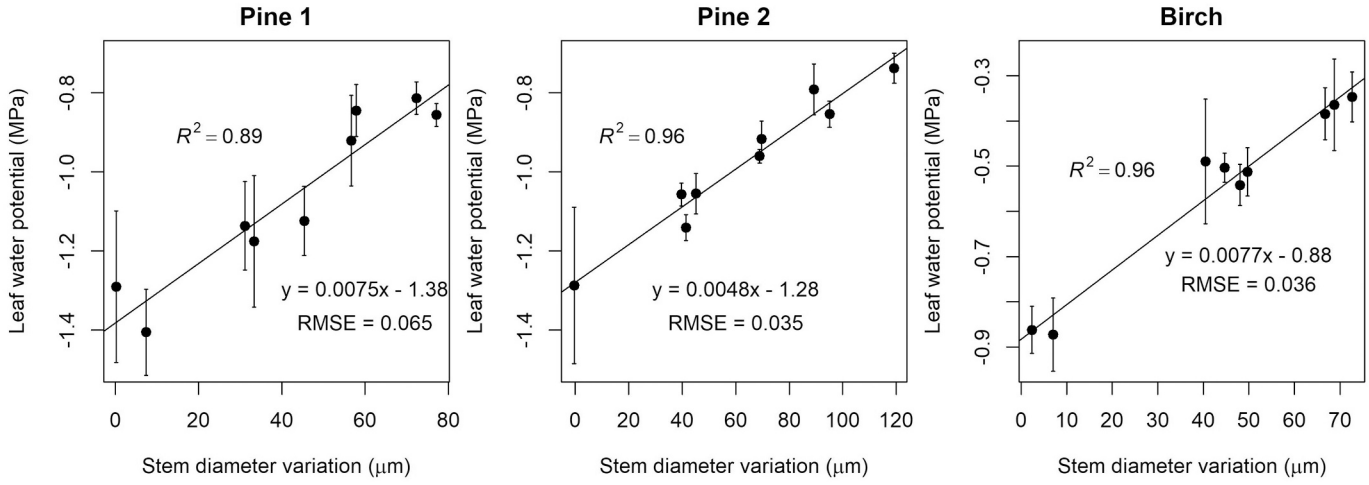

Fig. 3. The relationship between leaf water potential (Ψ_L) and stem diameter variation. The error bars represent the standard deviation of the Ψ_L measurements from different heights (each point is a mean of 12 observations). Coefficient of determination (R^2) and root-mean-square-error (RMSE) for the prediction models are also presented.

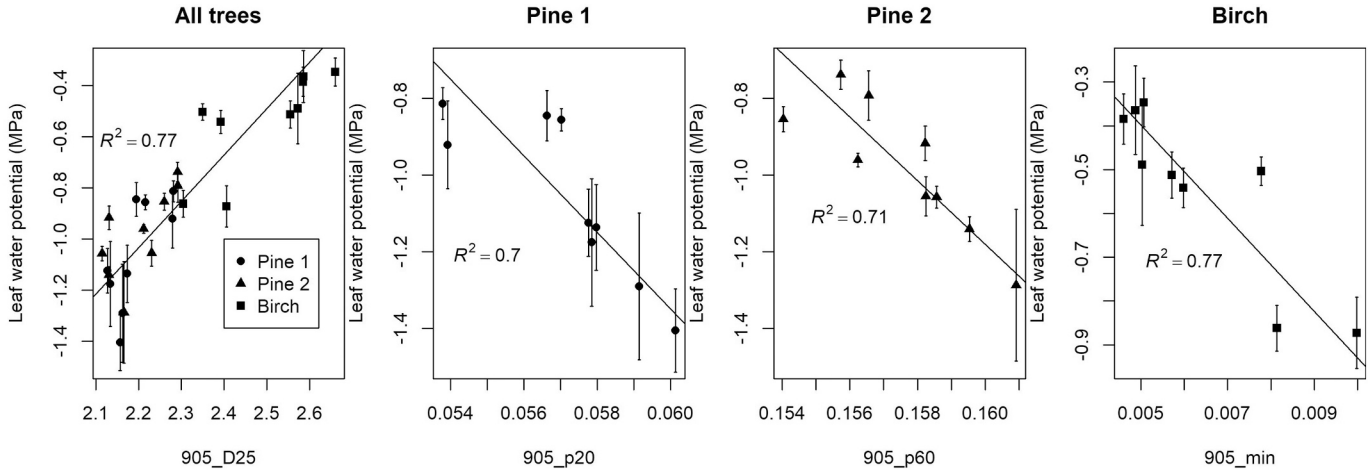

Fig. 4. The relationship and coefficient of determination (R^2) between leaf water potential (Ψ_L) and intensity metrics for all trees and for each tree separately. The error bars represent the standard deviation of measured Ψ_L at different heights (each point is a mean of four observations). Descriptions of the predictors 905_D25, 905_p20, 905_p60, and 905_min is provided in Table 2.

Table 3
The five strongest predictors, coefficient of determination (R^2), and root-mean-square-error (RMSE, MPa) for the linear regression models explaining leaf water potential (Ψ_L) using intensity metrics for each tree and all trees together. In these prediction models, Ψ_L and TLS intensity were measured at nine observation points in time. A description of the predictors is provided in Table 2.

Pine 1			Pine 2			Birch		
Predictor	R^2	*RMSE*	*Predictor*	R^2	*RMSE*	*Predictor*	R^2	*RMSE*
905_p20	0.70	0.111	905_p60	0.71	0.089	905_min	0.77	0.089
1550_p60	0.65	0.119	905_p50	0.71	0.089	1550_min	0.70	0.102
905_p30	0.65	0.120	905_p40	0.71	0.089	905_p05	0.65	0.109
1550_p70	0.62	0.124	905_mean	0.66	0.097	905_p10	0.60	0.117
1550_p80	0.56	0.134	905_p70	0.66	0.097	905_D25	0.53	0.128

All trees		
Predictor	R^2	*RMSE*
905_D25	0.77	0.141
905_D05	0.58	0.189
905_std	0.58	0.190
905_D50	0.55	0.196
905_p95	0.54	0.199

observations from all trees in the same model were not normally distributed, which is against the assumptions of linear regression, likely causing overestimation of the relationship. This was due to the uneven distribution of tree species in the samples.

3.4. Assessing the relationships between predicted leaf water potential and intensity metrics

When we predicted Ψ_L for all the 15 observation points in time (See 3.2) and used $\Psi_{P\text{-}L}$ as a dependent variable in our linear regression models, we obtained similar results as those presented in 3.3. On average, the 905 nm wavelength features were able to explain a larger proportion of the variation in predicted Ψ_L than the 1550 nm and NDI features with the exception of pine 1 (Table 4, Fig. 5). For the birch, the lowest part of the 905 nm intensity distribution was most sensitive to variation in Ψ_L with the 905_min, 905_p05, and 905_p10 features among the strongest predictors. Whereas the strongest predictors for the pines varied around the mean of the intensity distribution (i.e., p30, p40, p50, p60 features). Again we note that the intensity variables of all the trees pooled together were not normally distributed according to the Shapiro-Wilkinson test due to the different numbers of pines and birch in the data.

4. Discussion

The main aim of this study was to investigate how much of the diurnal variation in Ψ_L within Scots pine and silver birch trees can be explained using TLS intensity measurements. Our results showed that TLS intensity at both 905 nm and 1550 nm wavelengths increased due to decreased leaf water content, and that a time series of TLS intensity measurements can capture from 70% to 77% of the variation in measured Ψ_L for individual trees. Our destructive Ψ_L measurements were complemented with estimated Ψ_L values that were based on stem diameter change measurements and existing knowledge on the time lag between the change in Ψ_L and stem diameter (Lintunen et al., 2020). The time lag of 90 min that we used is in line with earlier results (Sevanto et al., 2002).

TLS intensity showed a relatively strong relationship with Ψ_L (R^2 of 0.56–0.77) for individual trees, especially at the 905 nm wavelength (See Table 3). This result is partly contrary to previous research, since the 1550 nm wavelength has been shown to be generally more sensitive to leaf water content than the 905 nm wavelength (Ceccato et al., 2001). Although the 905 nm wavelength can exhibit changes due to leaf water content (Penuelas et al., 1997), other factors may have contributed to the behaviour of the 905 nm wavelength in this study.

The amount of water in leaves is linked to their leaf area (Juneau and

Table 4
The five strongest predictors, coefficient of determination (R^2), and root-mean-square-error (RMSE, MPa) for the linear regression models explaining predicted leaf water potential ($\Psi_{P\text{-}L}$) using intensity metrics for each tree and all trees together. In these prediction models, Ψ_L is estimated for 15 observation points in time and the TLS intensities are measured from the respective time points. A description of the predictors is provided in Table 2. Note that predictor 905_D25 is transformed using a logarithm (log(905_D25)).

Pine 1			Pine 2			Birch		
Predictor	R^2	*RMSE*	*Predictor*	R^2	*RMSE*	*Predictor*	R^2	*RMSE*
1550_p50	0.56	0.170	905_p40	0.58	0.139	905_min	0.74	0.109
905_D75	0.53	0.175	905_entropy	0.58	0.139	905_p05	0.64	0.127
1550_p40	0.53	0.176	905_mean	0.56	0.142	905_entropy	0.63	0.131
1550_p30	0.50	0.182	905_p30	0.56	0.143	905_p10	0.62	0.132
1550_p60	0.49	0.182	1550_D50	0.53	0.146	905_p20	0.50	0.151

All trees		
Predictor	R^2	*RMSE*
log(905_D25)	0.70	0.180
905_D50	0.49	0.236
905_D05	0.47	0.241
905_std	0.47	0.242
NDI_p90	0.46	0.244

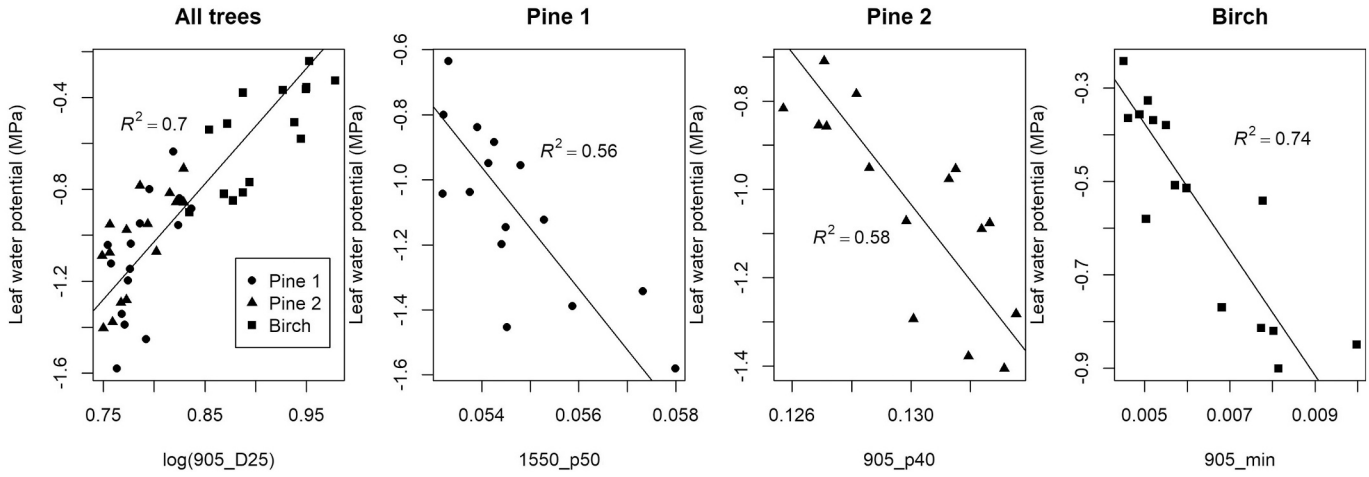

Fig. 5. The relationship and coefficient of determination (R^2) between predicted leaf water potential ($\Psi_{P\text{-}L}$) and laser intensity metrics for all trees and for each tree separately. A description of predictors 905_D25, 1550_p50, 905_p40, 905_min is provided in Table 2. The prefix log indicates that the predictor has been transformed using the logarithm function.

Tarasoff, 2012), thus, variation in the size of needles or leaves could have resulted in variation in TLS intensity. Another possible factor that could have co-occurred with changes in leaf water content is variation in leaf angle distribution. Reduced amount of water within leaves also affects their mass, which can affect the angle of leaves and needles relative to the branches holding them. In addition, diurnal branch movement has been detected using TLS and it could also affect the TLS intensity distribution of tree canopies within diurnal time scales (Puttonen et al., 2016). Since leaves tend to strongly reflect near-infrared light, where the 905 nm wavelength is situated, we could anticipate that any changes in the dimensions or angles of leaves would affect the 905 nm wavelength more than the 1550 nm wavelength. On the other hand, the TLS intensity difference between foliage and stem returns is greater for the 1550 nm wavelength, which is largely affected by water content (Ceccato et al., 2001; Feret et al., 2019). The stem points showed a two-fold higher reflectance compared to foliage points for the 1550 nm wavelength (average TLS intensity of needles 0.12 vs. 0.37 for the stem), but little difference was found between the two for the 905 nm wavelength (average TLS intensity of needles 0.31 vs. 0.45 for the stem). Thus, any change in the distribution of stem and foliage points within a sample caused, for example by altered leaf angle distribution, would be seen as a greater change in the TLS intensity distribution of the 1550 nm wavelength than the 905 nm wavelength. Therefore, without measurements of the aforementioned factors, it is difficult to state if the relationships between TLS intensity and Ψ_L are found solely on changes in leaf water content, but further studies should address the interaction of TLS intensity and diurnal variation of canopy properties more in-depth. However, based on the observed relationship between Ψ_L and TLS intensity in the field, TLS intensity measurements seemed relatively insensitive to the constantly varying illumination conditions which, based on previous research, hinder the use of passive remote sensing methods for many forest monitoring applications (Cheng et al., 2014; Nichol et al., 2006).

When estimating Ψ_L, we observed differences in the performance of the intensity metrics between the tree species. For Scots pines, the intensity metrics that were strongest predictors in explaining variation in Ψ_L were found around the middle of the intensity distribution at both the 905 nm and 1550 nm wavelengths varying between the 20th and the 60th percentile of the distribution. For silver birch, the intensity metrics that were strongest predictors in explaining variation in Ψ_L were in the lowest part of the intensity distribution of both the 905 nm and 1550 nm wavelengths, the 905 nm wavelength showing distinctly better performance. The differences in the intensity metrics explaining the variation in Ψ_L between trees are likely due to the varying structure of the tree crowns, difference in leaf shape (coniferous vs. deciduous), and differences in the numbers of needle/leaf and stem/branch points in the segmented point clouds.

Our preliminary tests indicated that filtering of stray points and detailed segmentation of the point clouds caused the relationship between intensity and Ψ_L to substantially decrease, which was likely due to the effect of these procedures on the intensity distribution. Therefore, we suggest that caution should be used when filtering, segmenting, and classifying point clouds as these procedures can have a significant impact on the TLS intensity distribution, especially when using a time series of intensity observations from the same target, as we did in this study. This has not been reported before. Thus, further studies should investigate the link between the stability of intensity distributions and different point cloud modifications.

We used a simple segmentation of the canopy and did not separate leaf and stem points in this study. We also did not filter stray or "ghost" points that commonly result from the laser hitting the edges of a target (Eitel et al., 2010). Although the leaf material classification could be expected to improve the estimation accuracy of Ψ_L, the correlation between TLS intensity metrics and Ψ_L was already strong using the methods applied in this study. However, for operational applications that could be used to predict Ψ_L over time for a large number of trees in forests, robust methods for separating leaf points would be required. Our results are likely influenced by the large amount of intensity observations from each tree canopy, which results in a more stable intensity distribution than that achievable for individual branches or leaves. The trees were also scanned each time from the same position, which in principle should result in a nearly equal number of stem and leaf points in the point clouds.

Earlier studies have found that NDI metrics have been stronger predictors for EWT than single-wavelength metrics, because another wavelength has been able to normalize a part of the variation in TLS intensity caused by varying incidence angle and leaf structure (Elsherif et al., 2019b; Junttila et al., 2019; Junttila et al., 2018). In this study, the NDI metrics did not provide any improvement compared to single-wavelength metrics in estimating Ψ_L, which may be caused by differences in the design of this and other experiments. The main differences compared to previous studies were: 1) the utilization of a dense time series to monitor diurnal variation in leaf water status instead of single observations of different leaves or trees with varying leaf water content, 2) the non-destructive nature of the research design (i.e. same trees were measured multiple times), and 3) the estimation of Ψ_L instead of EWT. Thus, direct comparisons to previous studies should not be made. The reason why the NDI metrics did not perform as well as single-wavelength metrics in the estimation of Ψ_L was likely firstly caused by the nearly constant leaf/needle structure during the monitoring period, which reduces the need for leaf structural normalization with NDI metrics (Junttila et al., 2018). Another likely reason is that within the tree canopies the incidence angle of leaves and needles should stay relatively constant at the canopy-level, and therefore the single wavelength intensity features are less influenced by the incidence angle. Single-wavelength metrics have also been strong predictors of EWT for single species in a drying experiment (Junttila et al., 2016). Structural differences in foliage have a greater effect on intensity if a larger number of trees are monitored simultaneously. Secondly, despite the wind speed was low during the monitoring period, slight movements of the leaves and branches occurred between the subsequent scans at the 905 nm and 1550 nm wavelengths, which may affect the stability of the NDI metrics through the time series. Thirdly, we used TLS intensity to measure the change in leaf water content and to derive Ψ_L instead of direct EWT estimation.

However, in our controlled experiment, TLS intensity proved able to explain 61–78% of the within-tree and between-tree variation in Ψ_L. The best-performing intensity features were mainly density features of the 905 nm wavelength (905_D25, 905_D05, 905_D50) that describe the variation in TLS intensity within a tree canopy. In other words, the changes in the shape of the intensity distribution due to varying Ψ_L have been similar between trees and tree species, encouraging further studies towards developing a general model that could estimate Ψ_L using TLS intensity measurements. The finding that density features outperformed other TLS intensity features can be partly explained by the ability of density features in normalizing TLS intensity differences between trees arising from calibration issues, because the density features are not sensitive to the absolute position of the TLS intensity distribution. We should note that the numbers of trees and samples were rather limited in our study for evaluating the capability of TLS intensity time series in estimating Ψ_L for trees of varying ages, species, and structures growing in various ecoregions, but based on our results, a clear correlation appears to occur between TLS intensity and Ψ_L.

Non-destructive measurements of Ψ_L using TLS intensity at larger scales could be feasible in the future if technical challenges can be overcome, which would enable tree stress detection and the investigation of canopy water dynamics at larger scales. Despite the fairly strong agreement between Ψ_L and TLS intensity, the best performing intensity features varied among the three measured trees in our study, which a sign of mild inconsistency of the TLS intensity distributions between the trees. Terrestrial laser scanning intensity measurements require calibration (Kaasalainen et al., 2011; Kaasalainen et al., 2009), but the lack of reliable calibration methods hinders the use of TLS intensity information on a larger scale. Firstly, the main challenges remain in the distance and incidence angle calibrations of TLS intensity, which require development to allow more robust measurements in varying forest conditions. Current calibration methods are unable to account for the differences in backscattered reflectance that are caused by small targets that do not cover the laser footprint entirely. This should be especially considered when measuring coniferous species with needles, which tend to be smaller than the laser footprint, because the relationship between laser intensity and distance is determined by the target size and a smaller amount of backscattered light is received small targets (Korpela, 2017). Secondly, accurate classification of foliage from woody material is required for assessing the canopy reflectance directly instead of using TLS intensity value distribution features that include woody material. A rigorous intensity calibration method would pave the way towards applications in tree and plant stress detection using also laser scanning from moving platforms such as airborne or mobile laser scanning that would enable large-scale monitoring of Ψ_L using diurnal measurements, which are currently challenging. However, based on the results of this study and earlier work (Junttila et al., 2019), static TLS intensity measurements from tree crowns may reveal changes caused by e.g. altered water content despite the challenges in the calibration.

The theoretical background of the link between relative water content and Ψ_L is strong, but there are also certain limitations to the capability of leaf water content in explaining Ψ_L variation. The used estimation approach is based on the relationship between Ψ_L and relative water content. However, relative water content is not the only variable affecting Ψ_L and osmotic potential may also affect Ψ_L, especially at longer time intervals or during extreme events such as drought (Bartlett et al., 2012; Nobel, 1999). Therefore, for longer time intervals (for example, month, season, year), the estimation accuracy of Ψ_L using TLS intensity is likely constrained by the influence of changes in osmotic potential.

We investigated the capability of TLS intensity in capturing the diurnal variation of Ψ_L. Earlier studies that have utilized TLS intensity in plant water status estimation have concentrated on estimating EWT, which may vary greatly within tree canopies and is strongly related to leaf mass per area (LMA). Leaf mass per area varies greatly between species and within species depending on environmental conditions such as light and temperature (Poorter et al., 2009). Therefore, EWT is less useful in understanding plant water status compared to Ψ_L (Elsherif et al., 2019b; Junttila et al., 2019). Although intensity metrics explained a large part of the variation in Ψ_L in our controlled experiment including three trees, there is still limited knowledge on how consistent the relation between Ψ_L and intensity metrics is within and between the tree communities. Theoretically, TLS can measure tens of tree canopies with a single easy-to-repeat scan and the ability of estimating the Ψ_L of these canopies would enable the measurement of Ψ_L at unprecedented spatial and temporal scales, which may help us further understand the

movement of water within the soil-plant-atmosphere continuum and the effect of a warmer and drier climate on our ecosystems.

Declaration of Competing interest

None.

Acknowledgements

This work was supported by the Faculty of Agriculture and Forestry of the University of Helsinki, the Academy of Finland under [grant numbers 307362, 316096/320075, and 330422], and the Finnish Cultural Foundation.

Appendix 1

In this appendix we present the detailed schedule of the TLS and Ψ_L measurements and the model parameters that were used to correct for the logarithmic behaviour of the TLS intensity.

Table 1
The starting time for each round of TLS scans and whether leaf water potential was measured or not.

Scan number	Time	Date	Ψ_L was measured
1	13:00	29.7.2019	yes
2	15:20	29.7.2019	yes
3	18:35	29.7.2019	yes
4	21:30	29.7.2019	yes
5	06:12	30.7.2019	no
6	8:22	30.7.2019	yes
7	12:37	30.7.2019	yes
8	15:05	30.7.2019	yes
9	18:04	30.7.2019	no
10	19:09	30.7.2019	yes
11	21:37	30.7.2019	no
12	05:51	31.7.2019	yes
13	09:45	31.7.2019	no
14	12:22	31.7.2019	no
15	14:04	31.7.2019	no

Table 2
The polynomial model parameters used for distance correction of TLS intensity.

Trimble TX5						
Intercept	a_1	a_2	a_3	a_4	a_5	a_6
1826.5	−142.5	126.0	0.3037	−75.7555	65.4323	−1.75
a_7	a_8	a_9	a_{10}			
−19.41	8.4852	26.2545	−21.18			

FARO X330						
Intercept	a_1	a_2	a_3	a_4	a_5	a_6
1550.813	−214.561	167.473	−58.98	−54.93	121.396	−112.53
a_7	a_8	a_9	a_{10}			
51.282	1.697	−32.113	25.183			

References

Antonarakis, A.S., Richards, K.S., Brasington, J., Muller, E., 2010. Determining leaf area index and leafy tree roughness using terrestrial laser scanning. Water Resour. Res. https://doi.org/10.1029/2009wr008318.

Baluja, J., Diago, M.P., Balda, P., Zorer, R., Meggio, F., Morales, F., Tardaguila, J., 2012. Assessment of vineyard water status variability by thermal and multispectral imagery using an unmanned aerial vehicle (UAV). Irrig. Sci. https://doi.org/10.1007/s00271-012-0382-9.

Bartlett, M.K., Scoffoni, C., Sack, L., 2012. The determinants of leaf turgor loss point and prediction of drought tolerance of species and biomes: a global meta-analysis. Ecol. Lett. 15, 393–405. https://doi.org/10.1111/j.1461-0248.2012.01751.x.

Beer, C., Reichstein, M., Tomelleri, E., Ciais, P., Jung, M., Carvalhais, N., Rödenbeck, C., Arain, M.A., Baldocchi, D., Bonan, G.B., Bondeau, A., Cescatti, A., Lasslop, G., Lindroth, A., Lomas, M., Luyssaert, S., Margolis, H., Oleson, K.W., Roupsard, O., Veenendaal, E., Viovy, N., Williams, C., Woodward, F.I., Papale, D., 2010. Terrestrial gross carbon dioxide uptake: global distribution and covariation with climate. Science 329, 834–838. https://doi.org/10.1126/science.1184984.

Bei, R.D.E., de Bei, R., Cozzolino, D., Sullivan, W., Cynkar, W., Fuentes, S., Dambergs, R., Pech, J., Tyerman, S., 2011. Non-destructive measurement of grapevine water potential using near infrared spectroscopy. Aust. J. Grape Wine Res. https://doi.org/10.1111/j.1755-0238.2010.00117.x.

Ceccato, P., Flasse, S., Tarantola, S., Jacquemoud, S., Grégoire, J.-M., 2001. Detecting vegetation leaf water content using reflectance in the optical domain. Remote Sens. Environ. https://doi.org/10.1016/s0034-4257(01)00191-2.

Chan, T., Hölttä, T., Berninger, F., Mäkinen, H., Nöjd, P., Mencuccini, M., Nikinmaa, E., 2016. Separating water-potential induced swelling and shrinking from measured radial stem variations reveals a cambial growth and osmotic concentration signal. Plant Cell Environ. 39, 233–244. https://doi.org/10.1111/pce.12541.

Cheng, T., Riaño, D., Ustin, S.L., 2014. Detecting diurnal and seasonal variation in canopy water content of nut tree orchards from airborne imaging spectroscopy data using continuous wavelet analysis. Remote Sens. Environ. https://doi.org/10.1016/j.rse.2013.11.018.

Cochard, H., Coll, L., Le Roux, X., Améglio, T., 2002. Unraveling the effects of plant hydraulics on stomatal closure during water stress in walnut. Plant Physiol. 128, 282–290. https://doi.org/10.1104/pp.010400.

Cohen, Y., Alchanatis, V., Meron, M., Saranga, Y., Tsipris, J., 2005. Estimation of leaf water potential by thermal imagery and spatial analysis. J. Exp. Bot. 56, 1843–1852. https://doi.org/10.1093/jxb/eri174.

Colombo, R., Meroni, M., Marchesi, A., Busetto, L., Rossini, M., Giardino, C., Panigada, C., 2008. Estimation of leaf and canopy water content in poplar plantations by means of hyperspectral indices and inverse modeling. Remote Sens. Environ. https://doi.org/10.1016/j.rse.2007.09.005.

Cotrozzi, L., Couture, J.J., Cavender-Bares, J., Kingdon, C.C., Fallon, B., Pilz, G., Pellegrini, E., Nali, C., Townsend, P.A., 2017. Using foliar spectral properties to assess the effects of drought on plant water potential. Tree Physiol. 37, 1582–1591. https://doi.org/10.1093/treephys/tpx106.

Davis, J.C., Sampson, R.J., 1986. Statistics and data analysis in geology (Vol. 646). Wiley, New York.

Dai, A., 2013. Increasing drought under global warming in observations and models. Nat. Clim. Chang. https://doi.org/10.1038/nclimate1633.

Danson, F.M., Steven, M.D., Malthus, T.J., Clark, J.A., 1992. High-spectral resolution data for determining leaf water content. Int. J. Remote Sens. https://doi.org/10.1080/01431169208904049.

Dassot, M., Constant, T., Fournier, M., 2011. The use of terrestrial LiDAR technology in forest science: application fields, benefits and challenges. Ann. For. Sci. https://doi.org/10.1007/s13595-011-0102-2.

Davies, O.L., Goldsmith, P.L., 1976. Statistical Methods in Research and Production.

De Swaef, T., De Schepper, V., Vandegehuchte, M.W., Steppe, K., 2015. Stem diameter variations as a versatile research tool in ecophysiology. Tree Physiol. 35, 1047–1061. https://doi.org/10.1093/treephys/tpv080.

Dewez, T.J.B., Girardeau-Montaut, D., Allanic, C., Rohmer, J., 2016. Facets : a CLOUDCOMPARE plugin to extract geological planes from unstructured 3D point clouds. Int. Archiv. Photogram. https://doi.org/10.5194/isprs-archives-xli-b5-799-2016.

Dietrich, L., Zweifel, R., Kahmen, A., 2018. Daily stem diameter variations can predict the canopy water status of mature temperate trees. Tree Physiol. 38, 941–952. https://doi.org/10.1093/treephys/tpy023.

Eitel, J.U.H., Vierling, L.A., Long, D.S., 2010. Simultaneous measurements of plant structure and chlorophyll content in broadleaf saplings with a terrestrial laser scanner. Remote Sens. Environ. https://doi.org/10.1016/j.rse.2010.04.025.

Elsherif, A., Gaulton, R., Mills, J., 2018. Estimation of vegetation water content at leaf and canopy level using dual-wavelength commercial terrestrial laser scanners. Interf. Focus 8, 20170041. https://doi.org/10.1098/rsfs.2017.0041.

Elsherif, A., Gaulton, R., Mills, J., 2019a. Four dimensional mapping of vegetation moisture content using dual-wavelength terrestrial laser scanning. Remote Sens. 11, 2311. https://doi.org/10.3390/rs11192311.

Elsherif, A., Gaulton, R., Shenkin, A., Malhi, Y., Mills, J., 2019b. Three dimensional mapping of forest canopy equivalent water thickness using dual-wavelength terrestrial laser scanning. Agric. For. Meteorol. 276-277, 107627. https://doi.org/10.1016/j.agrformet.2019.107627.

Feret, J.B., le Maire, G., Jay, S., Berveiller, D., Bendoula, R., Hmimina, G., Cheraiet, A., Oliveira, J.C., Ponzoni, F.J., Solanki, T., de Boissieu, F., Chave, J., Nouvellon, Y., Porcar-Castell, A., Proisy, C., Soudani, K., Gastellu-Etchegorry, J.P., Lefevre-Fonollosa, M.J., 2019. Estimating leaf mass per area and equivalent water thickness based on leaf optical properties: potential and limitations of physical modeling and machine learning. Remote Sens. Environ. 231, 110959. https://doi.org/10.1016/j.rse.2018.11.002.

Gaulton, R., Danson, F.M., Ramirez, F.A., Gunawan, O., 2013. The potential of dual-wavelength laser scanning for estimating vegetation moisture content. Remote Sens. Environ. 132, 32–39. https://doi.org/10.1016/j.rse.2013.01.001.

Guo, J.S., Hultine, K.R., Koch, G.W., Kropp, H., Ogle, K., 2020. Temporal shifts in iso/anisohydry revealed from daily observations of plant water potential in a dominant desert shrub. New Phytol. 225, 713–726. https://doi.org/10.1111/nph.16196.

Hanusz, Z., Tarasińska, J., 2015. Normalization of the Kolmogorov–Smirnov and Shapiro–Wilk tests of normality. Biomet. Lett. https://doi.org/10.1515/bile-2015-0008.

Hellkvist, J., Richards, G.P., Jarvis, P.G., 1974. Vertical gradients of water potential and tissue water relations in Sitka spruce trees measured with the pressure chamber. J. Appl. Ecol. https://doi.org/10.2307/2402215.

Juneau, K.J., Tarasoff, C.S., 2012. Leaf area and water content changes after permanent and temporary storage. PLoS One 7, e42604. https://doi.org/10.1371/journal.pone.0042604.

Junttila, S., Vastaranta, M., Liang, X., Kaartinen, H., Kukko, A., Kaasalainen, S., Holopainen, M., Hyyppä, H., Hyyppä, J., 2016. Measuring leaf water content with dual-wavelength intensity data from terrestrial laser scanners. Remote Sens. https://doi.org/10.3390/rs9010008.

Junttila, S., Sugano, J., Vastaranta, M., Linnakoski, R., Kaartinen, H., Kukko, A., Holopainen, M., Hyyppä, H., Hyyppä, J., 2018. Can leaf water content be estimated using multispectral terrestrial laser scanning? A case study with Norway spruce seedlings. Front. Plant Sci. 9, 299. https://doi.org/10.3389/fpls.2018.00299.

Junttila, S., Holopainen, M., Vastaranta, M., Lyytikäinen-Saarenmaa, P., Kaartinen, H., Hyyppä, J., Hyyppä, H., 2019. The potential of dual-wavelength terrestrial lidar in early detection of Ips typographus (L.) infestation – leaf water content as a proxy. Remote Sens. Environ. 231, 111264. https://doi.org/10.1016/j.rse.2019.111264.

Kaasalainen, S., Hyyppa, H., Kukko, A., Litkey, P., Ahokas, E., Hyyppa, J., Lehner, H., Jaakkola, A., Suomalainen, J., Akujarvi, A., Kaasalainen, M., Pyysalo, U., 2009. Radiometric calibration of LIDAR intensity with commercially available reference targets. IEEE Trans. Geosci. Remote Sens. https://doi.org/10.1109/tgrs.2008.2003351.

Kaasalainen, S., Jaakkola, A., Kaasalainen, M., Krooks, A., Kukko, A., 2011. Analysis of incidence angle and distance effects on terrestrial laser scanner intensity: search for correction methods. Remote Sens. https://doi.org/10.3390/rs3102207.

Kankare, V., Räty, M., Yu, X., Holopainen, M., Vastaranta, M., Kantola, T., Hyyppä, J., Hyyppä, H., Alho, P., Viitala, R., 2013. Single tree biomass modelling using airborne laser scanning. ISPRS J. Photogramm. Remote Sens. https://doi.org/10.1016/j.isprsjprs.2013.08.008.

Klepper, B., 1968. Diurnal pattern of water potential in woody plants. Plant Physiol. 43, 1931–1934. https://doi.org/10.1104/pp.43.12.1931.

Konings, A.G., Rao, K., Steele-Dunne, S.C., 2019. Macro to micro: microwave remote sensing of plant water content for physiology and ecology. New Phytol. 223, 1166–1172. https://doi.org/10.1111/nph.15808.

Korpela, I., 2017. Acquisition and evaluation of radiometrically comparable multi-footprint airborne LiDAR data for forest remote sensing. Remote Sens. Environ. https://doi.org/10.1016/j.rse.2016.10.052.

Krooks, A., Kaasalainen, S., Kankare, V., Joensuu, M., Raumonen, P., Kaasalainen, M., 2014. Tree structure vs. height from terrestrial laser scanning and quantitative structure models. Silva Fennica. https://doi.org/10.14214/sf.1125.

Kubiske, M.E., Abrams, M.D., 1991. Seasonal, diurnal and rehydration-induced variation of pressure-volume relationships in Pseudotsuga menziesii. Physiol. Plant. https://doi.org/10.1034/j.1399-3054.1991.830116.x.

Liang, X., Kankare, V., Yu, X., Hyyppa, J., Holopainen, M., 2014. Automated stem curve measurement using terrestrial laser scanning. IEEE Trans. Geosci. Remote Sens. https://doi.org/10.1109/tgrs.2013.2253783.

Lintunen, A., Paljakka, T., Salmon, Y., Dewar, R., Riikonen, A., Hölttä, T., 2020. The influence of soil temperature and water content on belowground hydraulic conductance and leaf gas exchange in mature trees of three boreal species. Plant Cell Environ. 43, 532–547. https://doi.org/10.1111/pce.13709.

Martinez-Vilalta, J., Anderegg, W.R.L., Sapes, G., Sala, A., 2019. Greater focus on water pools may improve our ability to understand and anticipate drought-induced mortality in plants. New Phytol. 223, 22–32. https://doi.org/10.1111/nph.15644.

McDowell, N.G., Allen, C.D., 2015. Darcy's law predicts widespread forest mortality under climate warming. Nat. Clim. Chang. https://doi.org/10.1038/nclimate2641.

Nevalainen, O., Hakala, T., Suomalainen, J., Mäkipää, R., Peltoniemi, M., Krooks, A., Kaasalainen, S., 2014. Fast and nondestructive method for leaf level chlorophyll estimation using hyperspectral LiDAR. Agric. For. Meteorol. https://doi.org/10.1016/j.agrformet.2014.08.018.

Nichol, J., Hang, L.K., Sing, W.M., 2006. Empirical correction of low Sun angle images in steeply sloping terrain: a slope-matching technique. Int. J. Remote Sens. https://doi.org/10.1080/02781070500293414.

Nobel, P.S., 1999. Physicochemical & Environmental Plant Physiology. Academic Press.

Olsson, K.A., Milthorpe, F.L., 1983. Diurnal and spatial variation in leaf water potential and leaf conductance of irrigated peach trees. Funct. Plant Biol. https://doi.org/10.1071/pp9830291.

Penuelas, J., Pinol, J., Ogaya, R., Filella, I., 1997. Estimation of plant water concentration by the reflectance Water Index WI (R900/R970). Int. J. Remote Sens. https://doi.org/10.1080/014311697217396.

Poorter, H., Niinemets, Ü., Poorter, L., Wright, I.J., Villar, R., 2009. Causes and consequences of variation in leaf mass per area (LMA): a meta-analysis. New Phytol. https://doi.org/10.1111/j.1469-8137.2009.02830.x.

Puttonen, E., Briese, C., Mandlburger, G., Wieser, M., Pfennigbauer, M., Zlinszky, A., Pfeifer, N., 2016. Quantification of overnight movement of birch (*Betula pendula*) branches and foliage with short interval terrestrial laser scanning. Front. Plant Sci. 7, 222. https://doi.org/10.3389/fpls.2016.00222.

Pyörälä, J., Kankare, V., Vastaranta, M., Rikala, J., Holopainen, M., Sipi, M., Hyyppä, J., Uusitalo, J., 2018. Comparison of terrestrial laser scanning and X-ray scanning in measuring Scots pine (*Pinus sylvestris* L.) branch structure. Scand. J. Forest Res. https://doi.org/10.1080/02827581.2017.1355409.

R. Core Team, 2015. An Introduction to R. Samurai Media Limited.

Rallo, G., Minacapilli, M., Ciraolo, G., Provenzano, G., 2014. Detecting crop water status in mature olive groves using vegetation spectral measurements. Biosyst. Eng. 128, 52–68. https://doi.org/10.1016/j.biosystemseng.2014.08.012.

Santos, A.O., Kaye, O., 2009. Grapevine leaf water potential based upon near infrared spectroscopy. Sci. Agric. https://doi.org/10.1590/s0103-90162009000300001.

Savage, M.J., Wiebe, H.H., Cass, A., 1983. In situ field measurement of leaf water potential using thermocouple psychrometers. Plant Physiol. 73, 609–613. https://doi.org/10.1104/pp.73.3.609.

Scholander, P.F., Bradstreet, E.D., Hemmingsen, E.A., Hammel, H.T., 1965. Sap pressure in vascular plants: negative hydrostatic pressure can be measured in plants. Science 148, 339–346. https://doi.org/10.1126/science.148.3668.339.

Seddon, A.W., Macias-Fauria, M., Long, P.R., Benz, D., Willis, K.J., 2016. Sensitivity of global terrestrial ecosystems to climate variability. Nature 531(7593), 229–232. https://doi.org/10.1145/3308561.3353779.

Sevanto, S., Vesala, T., Peramaki, M., Nikinmaa, E., 2002. Time lags for xylem and stem diameter variations in a Scots pine tree. Plant Cell Environ. https://doi.org/10.1046/j.1365-3040.2002.00884.x.

Elson, E.L., 2001. A mathematical theory of communication. ACM SIGMOBILE mobile computing and communications review 5(1), 3–55. https://doi.org/10.1145/3308561.3353779.

Syvertsen, J.P., Levy, Y., 1982. Diurnal changes in citrus leaf thickness, leaf water potential and leaf to air temperature difference. J. Exp. Botany. https://doi.org/10.1093/jxb/33.4.783.

Trenberth, K.E., 2011. Changes in precipitation with climate change. Clim. Res. https://doi.org/10.3354/cr00953.

Wagner, W., Ullrich, A., Ducic, V., Melzer, T., Studnicka, N., 2006. Gaussian decomposition and calibration of a novel small-footprint full-waveform digitising airborne laser scanner. ISPRS J. Photogramm. Remote Sens. https://doi.org/10.1016/j.isprsjprs.2005.12.001.

Wheeler, T., von Braun, J., 2013. Climate change impacts on global food security. Science. https://doi.org/10.1126/science.1239402.

Yrttimaa, T., Saarinen, N., Luoma, V., Tanhuanpää, T., Kankare, V., Liang, X., Hyyppä, J., Holopainen, M., Vastaranta, M., 2019. Detecting and characterizing downed dead wood using terrestrial laser scanning. ISPRS J. Photogrammet. Remote Sens. 151, 76–90. https://doi.org/10.31219/osf.io/t2h8r.